

Dynamical Properties of Multi-Armed Global Spirals in Rayleigh-Bénard Convection

Xiao-jun Li¹, Haowen Xi² and J. D. Gunton¹

¹*Department of Physics, Lehigh University, Bethlehem, Pennsylvania 18015*

²*Department of Physics and Astronomy, Bowling Green State University, Bowling Green, Ohio*

43403

(Submitted 20 May 1996)

Abstract

Explicit formulas for the rotation frequency and the long-wavenumber diffusion coefficients of global spirals with m arms in Rayleigh-Bénard convection are obtained. Global spirals and parallel rolls share exactly the same Eckhaus, zigzag and skewed-varicose instability boundaries. Global spirals seem not to have a characteristic frequency ω_m or a typical size R_m , but their product $\omega_m R_m$ is a constant under given experimental conditions. The ratio R_i/R_j of the radii of any two dislocations (R_i, R_j) inside a multi-armed spiral is also predicted to be constant. Some of these results have been tested by our numerical work.

PACS numbers: 47.20.Bp, 47.54.+r, 47.20.Lz, 47.27.Te

Typeset using REVTeX

Global spirals and *spiral defect chaos* (SDC) as intrinsic patterns have been experimentally observed recently in Rayleigh-Bénard convection (RBC) [4,5,10]. These observations were rather surprising because they were carried out in a parametric region where the familiar parallel-roll pattern should be stable [3]. An explanation for the unexpected presence of global spirals or SDC, in place of parallel rolls, is still to be provided. So far theoretical attempts on understanding these intriguing patterns rely heavily on numerical solutions of either the generalized Swift-Hohenberg (GSH) model [6–8,12] or the truncated Navier-Stokes equations governing the fluid dynamics [9]. Although these numerical studies have reproduced experimental results qualitatively and quantitatively, very limited theoretical insights have been obtained. While the formation of SDC in the system has since received considerable attention [8,9], little effort has been given to determining the essential properties of a *single* spiral. It is far from clear whether a global spiral has a characteristic rotation frequency ω_m or a typical size R_m [2]. The knowledge of those properties, we believe, is necessary in order to describe the much more complicated SDC.

Recently major progress was made by Cross and Tu (CT) in this front [12]. Applying the *phase dynamics* method developed earlier in studying pattern formations in non-equilibrium systems [14,15], CT considered the dynamics of a spiral as the balance of two competitive motions: a radial phase-drifting of the rolls and an azimuthal climbing of the dislocation [12]. CT's results also imply that $\omega_m R_m$ is a constant under given experimental conditions, but they did not give an explicit expression for $\omega_m R_m$. Furthermore, CT demonstrated qualitatively that the rotation frequency ω_m of a spiral is not directly related to *mean flow*, which is induced by distortions of the convective rolls [13], although mean flow is necessary for the formation of the rotating spiral [6–9].

In this paper we focus on dynamical properties of *global* spirals. We extend CT's results in two respects: We first make a one-mode approximation for spirals [18] which leads to an explicit expression for $\omega_m R_m$; we also separate the phase fluctuations from the stable phase-drifting and calculate the phase diffusion coefficients. We test some of these formulas by our numerical solutions. Our results make it possible to discuss the dynamical properties of

global spirals in detail. We predict that, inside a stable multi-armed global spiral, the ratio of the radii of two dislocations is a constant under given experimental conditions. We also find that global spirals, concentric rings and parallel rolls have exactly the same Eckhaus, zigzag and skewed-varicose instability boundaries. Presumably there is a competition among the various attractors corresponding to these states, the nature of which requires further theoretical study.

To be concrete, we base our calculations on the two-dimensional generalized Swift-Hohenberg (GSH) model for RBC [13], which has been proven very successful in characterizing convective patterns under quite broad conditions [1]. Numerical solutions of the GSH model not only reproduce both global spirals and SDC but also resemble experimental results reasonably well [6–8]. In this model, the convective patterns are determined completely by an *order parameter* $\psi(\mathbf{r}, t)$ in two-dimensional space \mathbf{r} , which satisfies [13]

$$\partial_t \psi + \mathbf{U} \cdot \nabla \psi = \left[\epsilon - (\nabla^2 + 1)^2 \right] \psi - g\psi^3 + g_3(\nabla \psi)^2 \nabla^2 \psi, \quad (1)$$

where \mathbf{U} is the mean flow velocity given by $\mathbf{U} = \nabla \zeta \times \mathbf{e}_z$ while [13]

$$\left[\partial_t - \sigma(\nabla^2 - c^2) \right] \nabla^2 \zeta = g_m \mathbf{e}_z \cdot \left[\nabla(\nabla^2 \psi) \times \nabla \psi \right]. \quad (2)$$

In the GSH equations, the reduced Rayleigh number $\epsilon = 2.7824\epsilon_{\text{expt}}$, where $\epsilon_{\text{expt}} \equiv (Ra/Ra_c) - 1$ is the control parameter [6,8], in which Ra and Ra_c are the Rayleigh number and its critical value at onset [1]. Other parameters g , g_3 , c^2 , g_m and the fluid Prandtl number σ model the properties of the system and are all non-negative. For simplicity, we only consider Oberbeck-Boussinesq fluids here [20].

A one-mode approximation has been used in studying spirals in chemical reaction-diffusion systems [18]. We now apply the same approximation for stable global spirals in RBC. Using polar coordinates (r, φ) , one can approximate a global-spiral solution by [20]

$$\psi(\mathbf{r}, t) = \frac{1}{2} \left[A_m(r) e^{i\theta_m} + \text{c.c.} \right] + O(A_m^3), \quad (3)$$

where $\theta_m = k_m(r)r + m\varphi - |m|\omega_m t$ with m the number of spiral arms near the core. In general, the amplitude $A_m(r)$ and the wave number $k_m(r)$ should depend on r . The rotation

frequency ω_m , however, must be independent of r for a stable spiral. Here we adopt the following conventions: $k_m(r) > 0$, $m > 0 (< 0)$ if the spiral is right(left)-handed and $\omega_m > 0 (< 0)$ if the spiral rotates in the same (opposite) direction of chirality. Experiments [4,10] showed that a multi-armed spiral usually has dislocations at different radii. Across each of these radii, the number of arms decreases or increases (depending on whether $m > 0$ or $m < 0$) by the number of dislocations on the corresponding radius. For mathematical simplicity, we denote each of these radii, for example R_i , by the number of non-terminating arms, say i , in its inside vicinity: See Fig. 1 for a $m = 3$ global spiral. Then a multi-armed spiral with dislocations at different radii can also be described by the above solution, provided that m is replaced by i for each corresponding region $R_j < r \leq R_i$. The amplitude and the wave number should be continuous across each boundary $r = R_i$. The frequency, on the hand, must be a constant for all regions. For $r > R_1$, only concentric rings (a target state) exist which corresponds to $i = 0$. With this understanding, our results below can be directly extended, by replacing m with every possible i , to multi-armed spirals found in experiments.

Phase equation [14,15] describes slow variations of convective rolls from their perfect pattern. Assuming $R_m \gg 1$, i.e., $\eta_m^2 \equiv 1/R_m \ll 1$ for a global spiral, one can then introduce *slow* scales $R \equiv \eta_m^2 r$, $\Phi \equiv \varphi$ and $T \equiv \eta_m^4 t$, and a *slow* phase variable $\Theta_m(\mathbf{R}, T) \equiv \eta_m^2 \theta_m(\mathbf{r}, t) + |m|\omega_m R_m T$. Here the phase fluctuations $\Theta_m(\mathbf{R}, T)$ have been explicitly separated from the stable phase-drifting $|m|\omega_m R_m T$. A similar separation has been used in studying chemical waves with steady velocity [1]. Now the local wave number can be defined as [14]

$$\mathbf{q}_m \equiv \nabla_{\mathbf{r}} \theta_m(\mathbf{r}, t) = \nabla_{\mathbf{R}} \Theta_m(\mathbf{R}, T) = q_m \mathbf{e}_r + O(\eta_m^2). \quad (4)$$

Inserting the spiral solution (3) into the GSH equation (1), one may then match the result to order η_m . Since the calculations are carried out in exactly the same way as in Ref. [14], we skip details here but only write down the final results. From the zeroth order of η_m , one finds that the amplitude is slaved by the wave number and is given by [19]

$$|A_m|^2 = 4 \frac{\epsilon - (1 - q_m^2)^2}{3g + g_3 q_m^4}. \quad (5)$$

From the second order of η_m , one obtains essentially the phase equation

$$\begin{aligned}\partial_T \Theta_m &= |m| \omega_m R_m - |A_m|^{-2} \nabla_{\mathbf{R}} \cdot [B(q_m) |A_m|^2 \mathbf{q}_m] \\ &\quad - \mathbf{U}' \cdot \mathbf{q}_m - g_3 q_m^{1/2} \mathbf{q}_m \cdot \nabla_{\mathbf{R}} [q_m^{3/2} |A_m|^2],\end{aligned}\tag{6}$$

where

$$B(q_m) = 2(1 - q_m^2) - \frac{3}{4} g_3 q_m^2 |A_m|^2,\tag{7}$$

while $\mathbf{U}' = \nabla_{\mathbf{R}} \langle \zeta \rangle_{\theta_m} \times \mathbf{e}_z$ with $\langle \cdots \rangle_{\theta_m}$ for the phase average in θ_m and, with $g'_m = g_m/c^2 \sigma$,

$$\nabla_{\mathbf{R}}^2 \langle \zeta \rangle_{\theta_m} = -\frac{1}{2} g'_m \mathbf{e}_z \cdot \mathbf{q}_m \times \nabla_{\mathbf{R}} [\nabla_{\mathbf{R}} \cdot (\mathbf{q}_m |A_m|^2)].\tag{8}$$

Although one may, in principle, convert Eq. (6) into the standard form as in Ref. [14], there is no need to do so here.

To express the phase equation in the more familiar diffusion equation form, one needs to project the gradient operator ∇ into local coordinates. In the light of Eq. (4), this can be easily achieved by $\partial_{\parallel} = \partial_R$ and $\partial_{\perp} = R^{-1} \partial_{\Phi} \simeq \partial_{\Phi}$ (since $R \simeq 1$ for $r \simeq R_m$ where the phase equation is valid). Again recalling Eq. (4), one finds immediately that $\nabla_{\mathbf{R}} \cdot \mathbf{q}_m = \nabla_{\mathbf{R}}^2 \Theta_m$. In Cartesian coordinates, this simply gives $\partial_{\parallel}^2 \Theta_m + \partial_{\perp}^2 \Theta_m$ which contributes to the diffusion of phase fluctuations. But in a polar coordinate system, an additional $R^{-1} \partial_{\parallel} \Theta_m \simeq q_m$ term is also present which, however, contributes to the stable phase-drifting $|m| \omega_m R_m T$! From Eq. (6), one gets via this $R^{-1} \partial_{\parallel} \Theta_m \simeq q_m$ term that [19]

$$|m| \omega_m R_m = q_m B(q_m),\tag{9}$$

whose corrections are of order η_m^2 . Apparently this frequency of rotation is generated by the curvature of convective rolls although it appears independent of mean flow. For $m = 0$, it naturally leads to the “wave number selection” $q_0 = q_f$ with $B(q_f) = 0$ [14,15].

Further algebra reduces Eq. (6) to a phase diffusion equation [14,17]

$$\partial_T \Theta_m = D_{\parallel}(q_m) \partial_{\parallel}^2 \Theta_m + D_{\perp}(q_m) \partial_{\perp}^2 \Theta_m + D_{\times}(q_m) \nabla_{\mathbf{R}}^{-2} \partial_{\parallel}^2 \partial_{\perp}^2 \Theta_m,\tag{10}$$

in which the diffusion coefficients are [19]

$$D_{\parallel}(q_m) = -\frac{1}{2}q_m \left[4\frac{1-q_m^2}{|A_m|^2} - g_3 q_m^2 \right] \frac{d}{dq_m} |A_m|^2 - B(q_m) + 4q_m^2, \quad (11)$$

$$D_{\perp}(q_m) = -B(q_m) + \frac{1}{2}g'_m q_m^2 |A_m|^2, \quad (12)$$

$$D_{\times}(q_m) = \frac{1}{2}g'_m q_m^3 \frac{d}{dq_m} |A_m|^2. \quad (13)$$

This diffusion equation describes three types of long-wave-length fluctuations [14,17]: Eckhaus (D_{\parallel}), zigzag (D_{\perp}) and skewed-varicose (D_{sv}) with, for $D_{\times} < 0$,

$$D_{sv}(q_m) = \left[(D_{\parallel} - D_{\perp})^2 + 2(D_{\parallel} + D_{\perp})D_{\times} + D_{\times}^2 \right] / 4D_{\times}. \quad (14)$$

When all these diffusion coefficients are positive, global spirals are stable; but when any one of them becomes negative, spirals lose their stability against the corresponding fluctuations.

One striking feature of this diffusion equation is that all the functions D_{\parallel} , D_{\perp} and D_{sv} are *independent* of m . Indeed they all agree with those of parallel rolls. This means that global spirals, concentric rings and parallel rolls share exactly the same Eckhaus, zigzag and skewed-varicose instability boundaries. So the fact that the measured wave numbers of stable spirals are inside the stable region of parallel rolls [4] is not surprising but necessary. Considering that the system is *non-potential* and that the only difference between spirals of different number of arms is q_m , a theoretical understanding of spiral-to-target or spiral-to-spiral transitions could be subtle. There are, however, some shortcomings in our analysis. The core instability [12] is omitted here. Short-wavelength fluctuations [3,17] have also been neglected, but these seem irrelevant in the transition between global spirals of different value of m [4,10]. In any event, it is clear that further theoretical work on this issue is necessary.

We now concentrate on the rotation frequency of the global spirals. One sees easily from Eq. (9) that $\omega_m R_m$ is a constant under given experimental conditions. This has been implied by CT [12] and verified by experiments [11] and our numerical solutions: see Table I. The quantitative value of $\omega_m R_m$ apparently depends on q_m . However, except for $m = 0$, one cannot determine q_m merely from the phase equation. This problem has been emphasized by CT [12]. They found that it is essential to take the intrinsic defect of the spiral, i.e., the

dislocation defect, into account. A spiral can be stable only if the phase-drifting of the rolls is balanced by the climbing of the dislocation, i.e., $\omega_m R_m = v_d(q_m)$, where $v_d(q_m)$ is the climbing velocity of the dislocation. This, together with Eq. (9), selects the wave number for a stable spiral. Unfortunately, an explicit analytic formula of $v_d(q_m)$ seems intractable [16]. Thus an accurate evaluation of q_m seems beyond reach.

One may still make the following approximations for small ϵ [12],

$$|m|\omega_m R_m \simeq \alpha(q_f - q_m), \quad v_d(q_m) \simeq \beta(q_m - q_d), \quad (15)$$

where $\alpha, \beta > 0$ and q_d is defined by $v_d(q_d) = 0$. For $g_3 = 0$, we get from Eq. (9) $q_f = 1$ and $\alpha = 4$, while for $g_3 > 0$, we get $q_f \approx 1 - \gamma_f \epsilon$ and $\alpha \approx 4(1 + \tilde{\alpha}\epsilon)$ with $\gamma_f = 3g_3/4(3g + g_3)$ and $\tilde{\alpha} = 6\gamma_f + \frac{32}{3}\gamma_f^2$. Similarly, one may write $q_d \approx 1 - \gamma_d \epsilon$ and $\beta \approx \beta_0(1 + \tilde{\beta}\epsilon)$. Under these approximations, the selected wave number of a stable spiral is fully determined by $\omega_m R_m = v_d$, which gives, with $\gamma_m = (4\gamma_f + |m|\beta_0\gamma_d)/(4 + |m|\beta_0)$,

$$q_m \simeq (\alpha q_f + |m|\beta q_d)/(\alpha + |m|\beta) \approx 1 - \gamma_m \epsilon. \quad (16)$$

Then, from Eq. (9), one finds for $m \neq 0$ that

$$\omega_m R_m \simeq \frac{\alpha\beta}{\alpha + |m|\beta}(q_f - q_d) \approx \frac{4\beta_0(\gamma_f - \gamma_d)\epsilon}{4 + |m|\beta_0}. \quad (17)$$

For a multi-armed spiral with dislocations at different radii, since the frequency of rotation is a constant over the whole spiral, the ratio $R_i/R_j = (\alpha + |j|\beta)/(\alpha + |i|\beta)$ is fixed under given experimental conditions. (The definition of R_i and R_j is given below Eq. (3).) This ratio depends on only two experimentally measurable quantities α and β [11], which provides a strong test of our theory.

To test the validity of Eq. (9), we have solved Eqs. (1) and (2) numerically by the same method described in Ref. [6], except that we set up a global spiral as the initial condition. We use $g = 1.0$, $g_3 = 0$, $\sigma = 1.0$, $c^2 = 2.0$ and $g_m = 10$ for our numerical solutions. We use mesh points $N \times N = 512 \times 512$ and grid size $\Delta x = \Delta y = \pi/8$ for aspect ratio (radius/thickness) $\Gamma = 32$. For simplicity, we set all radii of dislocations inside a multi-armed spiral to be equal. For $\epsilon = 0.3$, a one-armed spiral shrinks rapidly into concentric

rings. But for $\epsilon = 0.5$, one-armed, two-armed and three-armed spirals all stabilize with three given sizes $R_m/L = 0.45, 0.55, 0.65$ where $L = 32\pi$ is the radius of the cell. We then measure the rotation frequency and, via Eq. (9), calculate the corresponding wave number q_m . The results are listed in Table I. Although R_m varies by about 50%, the product $\omega_m R_m$ is found to be a constant within 5%. Also from Eq. (17) and the measured values of $\omega_m R_m$, we find that $\beta = 0.73 \pm 0.08$ and $q_d = 0.880 \pm 0.001$. In comparison, one gets $q_d \simeq 0.905$ from a formula in Ref. [16]. Furthermore, although global spirals are set up with three different sizes, they are all found to be stable within the time of our computer simulation, which runs about 2000 vertical diffusion times for each case. So it seems that global spirals do not have a typical size. Consequently, the frequency of rotation may also be non-unique.

Finally we make a comment on the role played by mean flow in the dynamics of spirals. Evidently Eq. (9) does not explicitly depend on g_m . This has been first observed by CT [12], who hence assign a “secondary” role to mean flow. Nevertheless mean flow plays a subtle role in determining the selected wave number (16) for *stable* spirals. Indeed the value of $q_f - q_d$ in Eq. (17) is very sensitive to g_m [16]. So $\omega_m R_m$ also has a sensitive g_m dependence. Furthermore, one must have $D_\perp \geq 0$ for stable spirals. This, from Eqs. (12) and (9), gives a constraint on the allowed frequency. For $g_m = 0$, only $\omega_m R_m \leq 0$ is permitted. Now if $\omega_m R_m \geq 0$ is also necessary to avoid “unwinding” [12], stable spirals must be stationary. Recalling Eq. (17), a stationary spiral is possible only if $q_f = q_d$. For $g_3 = 0$ and $g_m = 0$, the relation $q_f = q_d$ indeed holds [16] and a stationary global spiral has been found [6]. But for more realistic $g_3 > 0$, these two wave numbers are in general unequal. So a finite g'_m is needed to observe any stable spiral, which might suggest why a low Prandtl number ($g'_m \sim 1/\sigma$) is necessary in experiments [4,5,10].

In summary, we have calculated the rotation frequency and the long-wavelength diffusion coefficients of global spirals. We find that global spirals have exactly the same Eckhaus, zigzag and skewed-varicose instability boundaries as parallel rolls and concentric rings. So a transition between these patterns presumably involves a competition among their various attractors. Although global spirals seem not to have a characteristic frequency or a typical

size, the product of them is a constant under given experimental conditions. The ratio of the radii of any two dislocations inside a multi-armed spiral is also predicted to be constant. Some of these results have been tested by our numerical solutions. Nevertheless, to fully understand the intriguing global-spiral pattern, an analysis of the core instability and a theory describing the spiral-to-target transition will be necessary.

XJL and JDG are grateful to the National Science Foundation for support (under Grant No. DMR-9596202). Numerical calculations reported here are carried out on the Cray-C90 at the Pittsburgh Supercomputing Center and Cray-YMP8 at Ohio Supercomputer Center.

REFERENCES

- [1] M. C. Cross and P. C. Hohenberg, Rev. Mod. Phys. **65**, 851 (1993).
- [2] G. Ahlers, *Over Two Decades of Pattern Formation, A Personal Perspective* [preprint].
- [3] F. H. Busse, Rep. Prog. Phys. **41**, 1929 (1978).
- [4] E. Bodenschatz *et al.*, Phys. Rev. Lett. **67**, 3078 (1991); E. Bodenschatz *et al.*, Physica D **61**, 77 (1992).
- [5] S. W. Morris *et al.*, Phys. Rev. Lett. **71**, 2026 (1993).
- [6] H.-W. Xi, J. Viñals and J. D. Gunton, Phys. Rev. A **46**, R4483 (1992); H.-W. Xi, J. D. Gunton and J. Viñals, Phys. Rev. E **47**, R2987 (1993).
- [7] M. Bestehorn *et al.*, Phys. Lett. A **174**, 48 (1993).
- [8] H.-W. Xi, J. D. Gunton and J. Viñals, Phys. Rev. Lett. **71**, 2030 (1993); H.-W. Xi and J. D. Gunton, Phys. Rev. E **52**, 4963 (1995).
- [9] W. Decker, W. Pesch and A. Weber, Phys. Rev. Lett. **73**, 648 (1994).
- [10] B. B. Plapp and E. Bodenschatz [preprint].
- [11] E. Bodenschatz and B. B. Plapp, Bull. Am. Phys. Soc. **41**(1), 701 [Q18.8] (1996).
- [12] M. C. Cross and Y. Tu, Phys. Rev. Lett. **75**, 834 (1995).
- [13] J. Swift and P. C. Hohenberg, Phys. Rev. A **15**, 319 (1977); E. D. Siggia and A. Zippelius, Phys. Rev. Lett. **47**, 835 (1981); P. Manneville, J. Phys. (Paris) **44**, 759 (1983).
- [14] M. C. Cross and A. C. Newell, Physica D **10**, 299 (19984);
- [15] Y. Pomeau and P. Manneville, J. Phys. (Paris) **40**, L609 (1979); *ibid* **42**, 1067 (1981).
- [16] Y. Pomeau, S. Zaleski and P. Manneville, Phys. Rev. A **27**, 2710 (1983); G. Tesauero and M. C. Cross, *ibid* **34**, 1363 (1986).

- [17] H. S. Greenside and M. C. Cross, Phys. Rev. A **31**, 2492 (1985).
- [18] S. Koga, Prog. Theor. Phys. **67**, 164 (1982).
- [19] Following Pomeau and Manneville [15], an alternative method is to impose a small fluctuation $\phi(x, y, t)$ to the phase θ_m in Eqs. (1) and (3), and match the gradients $\nabla^n \phi$ order by order. This leads to the same results as cited in the text.
- [20] It is straight-forward to extend our calculation to the non-Oberbeck-Boussinesq case in which a $-g_2 \psi^2$ term will be added to Eq. (1). Consequently, in addition to mode (3), two extra modes $\frac{1}{2}(A_{m,0} + A_{m,2}e^{2i\theta_m} + \text{c.c.})$ are needed. Since these two extra modes are generated by the ψ^2 term, their amplitudes are both of order A_m^2 .

FIGURES

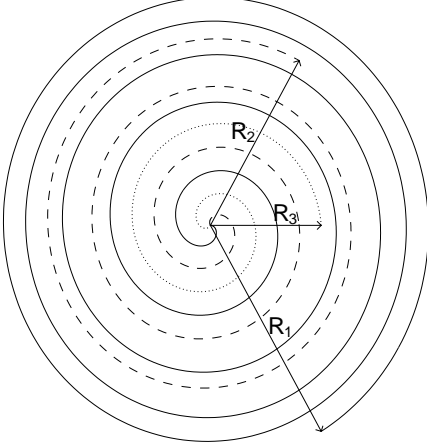


FIG. 1. Three-armed global spiral with dislocations at R_3 , R_2 and R_1 ($R_3 < R_2 < R_1$). The three arms are represented by the solid, dashed and dotted lines.

TABLES

TABLE I. Measured values of $\omega_m R_m$ of global spirals with $m = 1, 2, 3$ from numerical solutions. Global spirals are set up with three different sizes $R_m/L = 0.45, 0.55, 0.65$ where $L = 32\pi$ is the radius of the cell. The wave number q_m is calculated via Eq. (9), which is within the uncertainty of direct measurements $q_m = 1.00 \pm 0.05$.

| m | $R_m/32\pi$ | $\omega_m R_m$ | q_m |
|-----|-------------|----------------|-------|
| 1 | 0.45 | 0.0750 | 0.981 |
| | 0.55 | 0.0742 | 0.981 |
| | 0.65 | 0.0734 | 0.981 |
| 2 | 0.45 | 0.0619 | 0.967 |
| | 0.55 | 0.0630 | 0.967 |
| | 0.65 | 0.0658 | 0.965 |
| 3 | 0.45 | 0.0574 | 0.954 |
| | 0.55 | 0.0568 | 0.954 |
| | 0.65 | 0.0556 | 0.955 |